Efficient Computation for a Reaction-Diffusion System with a Fast Reaction in Two Spatial Dimensions Using COMSOL Multiphysics

Aaron Churchill, Matthias K. Gobbert, and Thomas I. Seidman

Department of Mathematics and Statistics, University of Maryland, Baltimore County

{achurc1,gobbert,seidman}@umbc.edu

Abstract

We study a reaction-diffusion system of three chemical species, where two chemicals react with a much faster rate than the other reaction in the model. We are interested in the asymptotic limit as the rate becomes infinite. This forces the reaction interface to have an asymptotically small width with asymptotically large height. Numerical simulations for the three species model with large reaction rate become progressively more challenging and costly as the singularity becomes sharper. But in the asymptotic limit, an equivalent two component model can be defined that is significantly cheaper computationally and allows for effective studies for the model. The equivalence is demonstrated by the analytical definition of the two component model and by comparing numerical results to ones for the three species model with progressively larger reaction rates, which also demonstrate the computational efficiency.

1 Introduction

Our objective is to study the diffusion controlled reactions

$$\mathrm{A} + \mathrm{B} \xrightarrow{\lambda} \mathrm{C}, \qquad \mathrm{A} + \mathrm{C} \xrightarrow{\mu} (*)$$

in the two-dimensional domain $\Omega := (0,1)\times(0,1) \subset \mathbb{R}^2$. In the reaction model, λ and μ are reaction coefficients with the units scaled such that $\lambda \gg \mu = 1$. We denote the concentrations of the three chemical species A, B, and C by $u(x,t)$, $v(x,t)$, and $w(x,t)$, respectively. Standard chemical kinetics then give a three species system of partial differential equations for these concentrations as

$$\left.\begin{array}{rcccccccc} u_t &=& u_{xx} &+& u_{yy} &-& \lambda uv &-& uw \\ v_t &=& v_{xx} &+& v_{yy} &-& \lambda uv & & \\ w_t &=& w_{xx} &+& w_{yy} &+& \lambda uv &-& uw \end{array}\right\} \text{ for } (x,y)\in\Omega \text{ and } t\in(0,t_{\mathrm{fin}}]. \tag{1.1}$$

The boundary conditions considered are

$$\left.\begin{array}{l} u = \alpha(y) \\ v_x = 0 \\ w_x = 0 \end{array}\right\} \text{along } x=0, \qquad \left.\begin{array}{l} u_x = 0 \\ v = \beta(y) \\ w_x = 0 \end{array}\right\} \text{along } x=1, \qquad \left.\begin{array}{l} u_y = 0 \\ v_y = 0 \\ w_y = 0 \end{array}\right\} \text{along } y=0 \text{ and } y=1. \tag{1.2}$$

This setup represents the case of a tank with unlimited supply of A to the left and a tank with unlimited supply of B to the right of the domain Ω. If the boundary condition functions are chosen as constants independent of y, that is, $\alpha(y) \equiv \alpha$ and $\beta(y) \equiv \beta$, then taking for each value of y the solution of the corresponding problem in one spatial dimension with domain $0 < x < 1$ clearly is a also a solution of the two-dimensional problem. This fact has already been used in [7] to confirm the validity of simulations for this two-dimensional generalization. Even while maintaining this restriction on the boundary conditions here, the model can show very interesting behavior as result of initial conditions that give a structure to the distribution of u and v in the interior of the domain. For physical intuition, we will consider initial conditions at $t = 0$ with species A and B present in separate regions, thus $u \geq 0$ and $v \geq 0$ with $uv = 0$, and the intermediate compound C not present at all throughout the domain, thus $w \equiv 0$. The functions u and v at $t = 0$ will be chosen consistent with the boundary conditions.

Singular perturbation analysis for the corresponding stationary problem in one spatial dimension is available in [1, 4], which prove the existence of an internal layer with width $\mathcal{O}(\varepsilon)$ and height $1/\mathcal{O}(\varepsilon)$ with scaling $\varepsilon = \lambda^{-1/3}$. The transient three species model in one spatial dimension has already been considered computationally in [2, 6]. Numerical studies on three initial conditions for the 1-D problem with continuous initial

conditions in [6] allow us to conclude that the moving, sharp, internal layer in the transient problem has the same scaling as in the stationary problem. Studies in [2] consider $\lambda = 10^6$ and 10^9 and lead us to conclude that both values are already in the asymptotic regime, which gives strong guidance as to what to expect from the problem in the asymptotic limit. The recent paper [3] introduces a two component model that is equivalent to the above three species model in the asymptotic limit $\lambda \to \infty$, but promises to be significantly more computationally efficient, since it lacks the sharp internal layer present in the three species model. The internal layers become implicit in the two component model, showing up as discontinuities in spatial derivatives for the original species rather than a term λuv in the equation.

We are interested in initial conditions such as is shown in Figure 1. Each connected piece of each initial

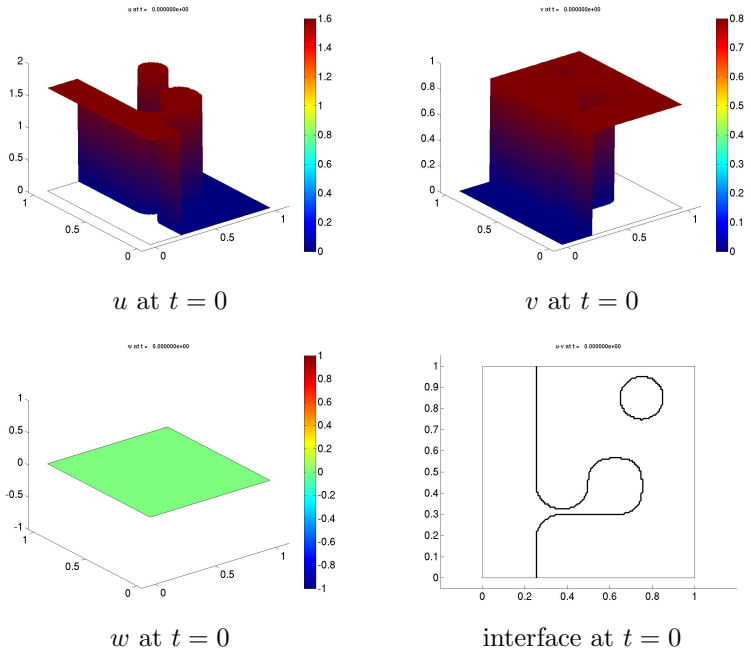

u at $t = 0$ v at $t = 0$

w at $t = 0$ interface at $t = 0$

Figure 1: Initial Condition for u, v, and w, and the initial interface.

concentration has some constant value. The left hand portion of the domain has values of $u = \alpha$ and $v = 0$ and the right hand portion has $u = 0$ and $v = \beta$. The small disk in the upper right of the domain has values $u = \alpha$ and $v = 0$. We use the values $\alpha = 1.6$ and $\beta = 0.8$ here. The concentration of w is 0 throughout the domain at $t = 0$. The fast reaction in the reaction model is restricted to areas of Ω where u and v co-exist. This is only the case along certain lines through the domain where u and v come in contact due to diffusion. We call these lines the reaction interface shown in the final plot in Figure 1. To allow us a concrete reference to various parts of the domain, we use the following terminology in the following: The portion on the left side of the domain is called the 'body,' and the piece protruding from the body is called the 'head,' which is connected to the body by the 'neck.' The inspiration for these terms is most evident in the image of the initial interface in Figure 1.

Our goals in this report are to present evidence that the two component model, first presented in [3] and then studied in both 1-D and 2-D in [7], is equivalent to the original three species model in 2-D and is computationally superior to the original three species model in 2-D. First in Section 2 we present a short analytical derivation of the two component model. Next, in Section 3.1, we graphically compare the progression of both the three species model and two component model over time from the initial conditions in Figure 1 for $\lambda = 10^3$, 10^6, 10^9, and ∞; we use the phrase $\lambda = \infty$ here and in the following as a short hand notation to indicate the use of the two component model. Finally in Section 3.2, we give numerical performance data and numerical accuracy data for various spatial resolutions for each of the above λ values.

2 The Two Component Model

Computationally, the greatest difficulty in handling the system (1.1) is the occurrence of $q = \lambda uv$ in each of the equations. Chemical modeling and the rigorous analysis available for the corresponding steady state system in 1-D show that this point wise reaction rate is very large where relevant — in a narrowly concentrated reaction zone: we expect this to be negligible where one or the other of A, B dominate, but to be significant where the diffusion transports these to meet each other at the interface and react rapidly there. For computation one needs fairly accurate determination of the integral of q so one must adequately resolve the q profile — a 'spike' in 1-D, a 'wall' in 2-D, etc. — with the further difficulty that the location of this 'spike' is not known a priori. Since the difference A − B and the sum B + C are each conserved in the first reaction, this difficult reaction term cancels when one combines the pairs of equations to get

$$\left.\begin{array}{l}(u-v)_t = (u-v)_{xx} + (u-v)_{yy} - uw \\ (v+w)_t = (v+w)_{xx} + (v+w)_{yy} - uw\end{array}\right\} \text{ for } (x,y) \in \Omega \text{ and } t \in (0, t_{\text{fin}}]. \tag{2.1}$$

The term q no longer appears explicitly, but the system (2.1) is no longer self-contained: we cannot recover the three species concentrations u, v, w from the two components

$$u_1 := u - v, \qquad\qquad u_2 := v + w \tag{2.2}$$

to determine the second reaction term uw. On the other hand, we always have $u, v \geq 0$ and in the limit $\lambda \to \infty$ we also have the complementarity condition

$$uv \equiv 0$$

(meaning that uv is negligible for large λ, even though, when this is multiplied by $\lambda \gg 1$, q can become large). Thus, in this limit, when $u_1 > 0$ we must have $u \neq 0$ so $v = 0$ and $u_1 = u$, while $u_1 < 0$ similarly gives $u = 0$ whence $u_1 = -v$. It then becomes possible to take

$$u = u_1^+ := \max\{u_1, 0\}, \qquad v = -u_1^- := -\min\{u_1, 0\}, \qquad w = u_2 + u_1^- \tag{2.3}$$

and so $uw = u_1^+(u_2 + u_1^-) = u_1^+ u_2$. The formulas in (2.2) and (2.3) in effect constitute forward and backward transformations between the three species and the two component models. The corresponding two component model is then

$$\left.\begin{array}{rcl}u_{1,t} &=& u_{1,xx} + u_{1,yy} - u_1^+ u_2 \\ u_{2,t} &=& u_{2,xx} + u_{2,yy} - u_1^+ u_2\end{array}\right\} \text{ for } (x,y) \in \Omega \text{ and } t \in (0, t_{\text{fin}}]. \tag{2.4}$$

We emphasize that this is exactly valid only in the limit, but is approximately correct for large λ. There is no difficulty in obtaining the initial conditions for the two components $u_1 = u - v$ and $u_2 = v + w$ from those given for u, v, w, but we must also adjoin boundary conditions for the two component system. For this, we again use (2.3), now in (1.2), to get

$$\left.\begin{array}{l}u_1 = \alpha \\ u_{2,x} = 0\end{array}\right\} \text{along } x = 0, \qquad \left.\begin{array}{l}u_1 = -\beta \\ u_{2,x} = -u_{1,x}\end{array}\right\} \text{along } x = 1, \qquad \left.\begin{array}{l}u_{1,y} = 0 \\ u_{2,y} = 0\end{array}\right\} \text{along } y = 0 \text{ and } y = 1, \tag{2.5}$$

so the complete two component system (2.4)–(2.5) becomes self-contained, although at the price of a rather unusual coupling in the second boundary condition along $x = 1$. Computationally, the two component model can be expected to be much easier to work with since the solutions are more regular: the derivative discontinuities of the species concentrations just match to make the derivatives of u_1 and u_2 continuous across the interfaces where the derivatives of u, v, and w are not.

This report explores precisely the relative computational efficiency of the two component model.

3 Comparison of the Three Species and Two Component Models

For the following computations, we use COMSOL Multiphysics 3.5a on the cluster hpc in the UMBC High Performance Computing Facility (`www.umbc.edu/hpcf`). COMSOL is run on one node with two dual-core AMD Opteron processors (2.6 GHz, 1 MB cache per core) and 13 GB of memory. We couple COMSOL with Matlab using the Linux command `comsol matlab`. With this, a script is written so that each computation would be using the same solver parameters inside COMSOL. We use linear Lagrange finite elements on a uniform $N \times N$ mesh. Observe that the default settings in COMSOL are an unstructured mesh which the solver computes with quadratic Lagrange finite elements. By using a structured, uniform mesh, we avoid any incidental biasing that might affect the solution as result of, e.g., some region of Ω having slightly more elements than another, from element boundaries being at non-horizontal or non-vertical angles, or similar properties inherent to an unstructured mesh. Because the solutions have jump discontinuities at the initial time and will have discontinuities in their derivatives at the reaction interfaces, we use the lowest order finite elements available in COMSOL. The ODE solver used is BDF-DASPK. This solver is chosen because BDF-IDA, the default solver, has trouble converging at the initial conditions for the case of large λ values. The ODE solver Generalized Alpha was also experimented with, but this too had some difficulties. While it allows the user to request only specific timesteps to be output, but might prevent the solver from using the optimal, fewest number of time steps, which is our goal here. We use a relative tolerance of 10^{-3} and an absolute tolerance of 10^{-6} for the local error control in the ODE solver. We use the linear solver PARDISO.

An interesting feature of this problem when used with COMSOL is the coupled boundary condition along $y = 1$. Many solvers have difficulty handling a boundary condition of this type. Additionally, we enter the PDE in General Form in COMSOL, which is designed for strongly non-linear problems, because it allows COMSOL to differentiate all terms symbolically (and not numerically) for the highest accuracy in the evaluation of the Jacobian in the non-linear solver inside the ODE method.

In this section, we present numerical results that offer evidence that the two component model is computationally superior to the three species model. First, we give evidence that over time both the three species model and two component model give equivalent results. Next, we give a numerical comparison of the two methods based on the grid size used in the computations. Recall that $\Omega = (0,1) \times (0,1)$ and $\alpha = 1.6$ and $\beta = 0.8$ in the initial conditions in Figure 1.

3.1 Graphical Comparisons

The following pages show a comparison over time of different λ values. For each of the values $\lambda = 10^3, 10^6, 10^9$, and ∞, we present images of u, v, w, and the reaction interface. For the $\lambda = \infty$ case, we back transform u_1 and u_2 into u, v and w using the transformations $u = \max\{u_1, 0\}$, $v = -\min\{u_1, 0\}$ and $w = u_2 - \min\{u_1, 0\}$ from (2.3). Each page shows the results at the six times $t = 10^{-4}, 10^{-3}, 10^{-2}, 10^{-1}$, 1, and 20. We see quickly that the interface plots show an incredible similarity in their evolutions. This is evident even in the $\lambda = 10^3$ case. All of these images were created using a 128×128 mesh of linear Lagrange elements.

Specifically, we discuss the results for $\lambda = 10^6$ in Figures 6, 7, 8, and 9 in detail now. Figures 6, 7, and 8 show the evolution over time of the chemical species u, v, and w, respectively for $\lambda = 10^6$. For example, we see in Figure 6 that over time, u starts from the initial condition in Figure 1 with $u = \alpha = 1.6$ along $x = 0$ and $u = 0$ along $x = 1$. Over a short period of time in the first frame of Figure 6, the sharp edges, which represent a sharp drop off in the amount of chemical, has rounded off as some of the chemical towards the edge reacts with some of the other chemical. As time progresses, we see that the mound has rounded off even more. In the next frame, the mounds have almost completely disappeared. In the last two frames, the chemical has just about settled into its steady state. There is a similar progression in the v images in Figure 7, with $v = 0$ along $x = 0$ and $v = \beta = 0.8$ along $x = 1$. In the w images in Figure 8, we see that the simulation starts with $w = 0$ throughout Ω in Figure 1 and that some $w > 0$ develops first along the reaction interfaces in the first frame of Figure 8. As time progresses in the next few frames, we see that the areas with less w start to fill in by diffusion from the reaction interface, which is the only place where w is generated. In the following two frames, the peak amount of w still follows the reaction interface. But eventually, the amount of w is highest in the right portion of the domain; this results from the fact that the intermediate species is consumed in a reaction with the first species u, but not the second v, hence it can diffuse from the reaction

interface to the right without consumption, while the concentration of w progressively decreases as it diffuses from the reaction interface to the left of the interface. We observe that the growth of w slows down over time towards an apparently finite steady state value; that is a significant observation, for which a rigorous proof is only being developed at present [5]. The most interesting set of images is the collection of interface images in Figure 9. We see here the outlines of the actual reaction interface where $u > 0$ and $v > 0$ meet by diffusion and react rapidly with rate λuv. Recall that at the initial time, these two species do not coexist and mathematically $uv = 0$. It is only by diffusion that positive values of both get in contact with each other and this gives the first positive values of the resulting reaction intermediate w. Numerically, we determine the location of the interface as a contour plot with one contour level of value 0 of the difference $u - v$. In the first frame of Figure 9 at $t = 10^{-4}$, we can still clearly see the 'head' connected by the 'neck' to the 'body' on the left portion of the domain and an disjoint 'disk' in the upper right of the domain, like in the initial condition in Figure 1; these outlines have the same shape as the locations of $w > 0$ at the corresponding time in Figure 8. In the next frame, we see the head separating from the body in the left portion of the domain, before it re-attaches to the body in the following frame. Also by the time of the third frame, the disjointed disk has vanished with its supply of the u species completely consumed. The chosen initial conditions give rise to an interesting behavior in that the head separates and then re-attaches to the body in the left portion of the domain, while at the same time the disk disappears. In the last three frames, we see the interface tends to its steady state location at $x^* \approx 0.6$.

Comparing the set of figures for $\lambda = 10^6$ to the corresponding ones for the other values of λ as well as the two component model with $\lambda = \infty$ in Figures 14, 15, 16, and 17, we can clearly see that the progression over time is essentially identical up to the graphical resolution of the studies.

3.2 Accuracy and Efficiency Comparisons

The graphical results in the figures in the previous section indicate that the two component model appears to give results that are qualitatively consistent with the three species model in the asymptotic limit of $\lambda \to \infty$. This section defines four measures to study the accuracy of the two component model quantitatively. As our goal in this report is to verify that the two component model is numerically superior to the three species model, we also define two measures to validate the efficiency quantitatively. The four measures of accuracy and two measures of efficiency are studied over a variety of finite element meshes with $N \times N$ elements.

The first measure of accuracy is the closeness of the location x^* of the interface at the final time of the transient problem to that of the actual steady state interface, which is $x^*_{\text{steady}} = 0.601806640625$; this value was obtained by simulations of the three species steady state problem in 1-D on a high resolution mesh with $N = 8{,}192$ and will be considered the true value for x^* in the following. The other measures of accuracy are three times t_1, t_2, and t_3 defined by significant transitions in the development of the interface plot. The time t_1 represents the time at which the head separates from the body in the left portion of the domain; t_2 represents the time at which the head re-attaches to the body, and t_3 represents the time at which the disjoint disk in the upper right of the domain dissipates. These times were obtained by viewing movies of the interface, where the movies were compiled using the output of all time steps from the ODE solver, which are substantially more than the six times in the figures. Thus the times listed are as precise as possible for each simulation, but are limited in accuracy by the number of time steps and their exact choice made by the time step selection algorithm in the ODE solver. The x^* values in Table 1 are identical for the $\lambda = 10^6$, 10^9, and ∞ cases. They are slightly different among the mesh resolutions, but within the mesh resolution to x^*_{steady} in each case. In $\lambda = 10^3$ case, the x^* values are slightly off, because they have not reached their asymptotic values, yet. We see in Table 1 that the corresponding times t_1, t_2, and t_3 are very close for all $\lambda = 10^3$, 10^6, 10^9, and ∞, for each fixed mesh resolution $N \times N$. The difference in the values of the times between different mesh resolutions is explained by the fact that they generate slightly different initial conditions, depending on how exactly the curved boundaries in the initial conditions are resolved, which result in slightly different behavior over time. Because the accuracy results are nearly identical across at least $\lambda = 10^6$, 10^9, and ∞ for each fixed mesh resolution, these accuracy measures confirm that the two component model ($\lambda = \infty$) is an accurate simulator for the three species model in the asymptotic limit.

As measures of efficiency, we consider the number of time steps taken by the ODE solver and the total

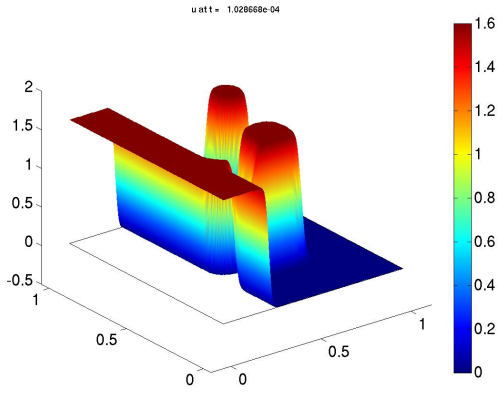

$t = 10^{-4}$

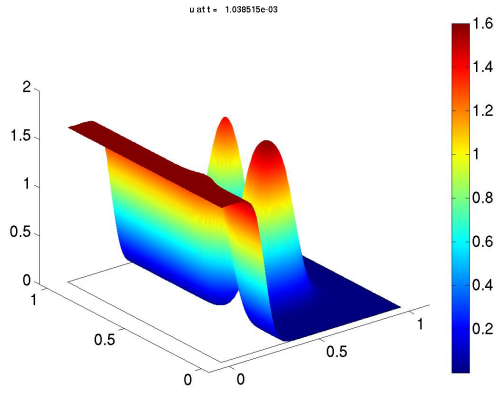

$t = 10^{-3}$

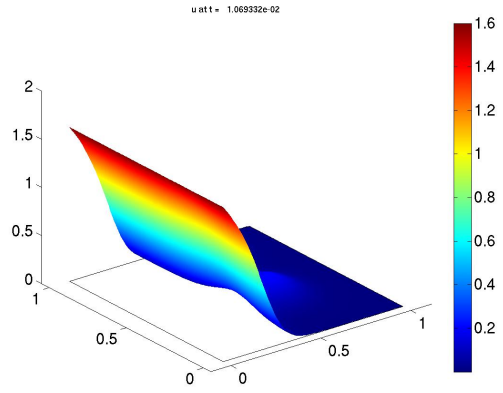

$t = 10^{-2}$

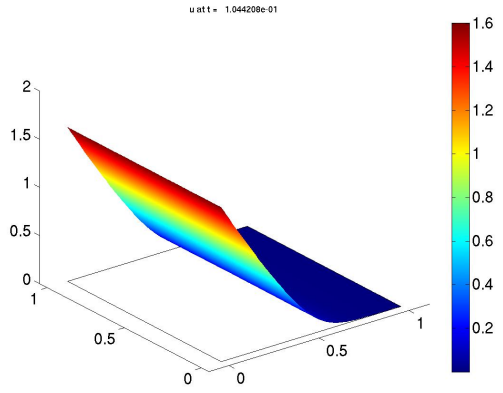

$t = 10^{-1}$

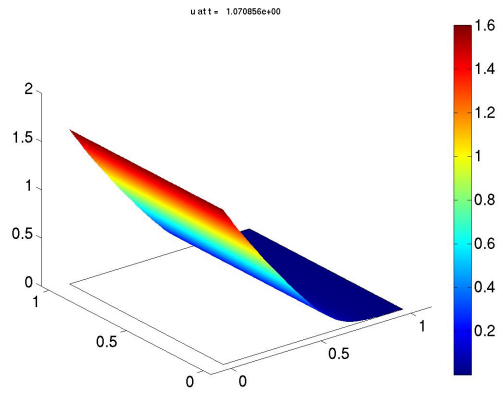

$t = 1$

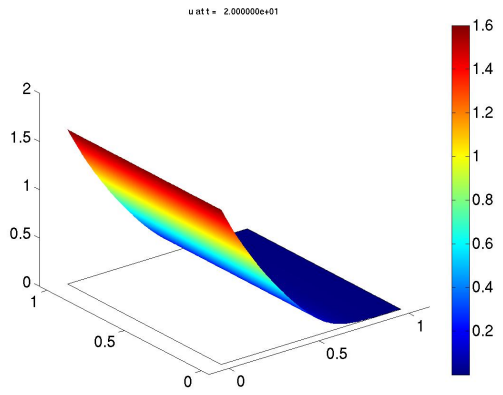

$t = 20$

Figure 2: $u(x, y, t)$ vs. (x, y) at specified times for $\lambda = 10^3$.

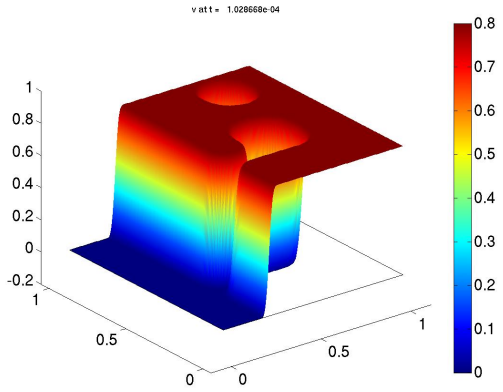

$t = 10^{-4}$

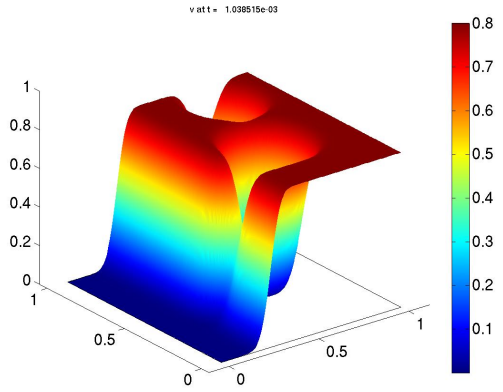

$t = 10^{-3}$

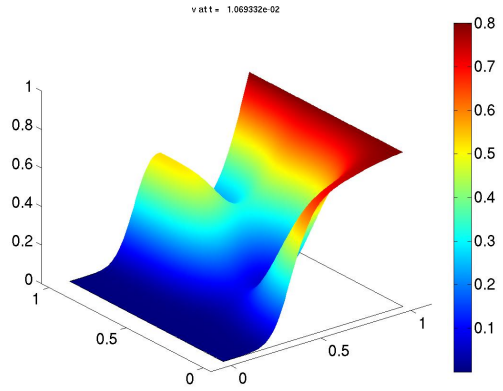

$t = 10^{-2}$

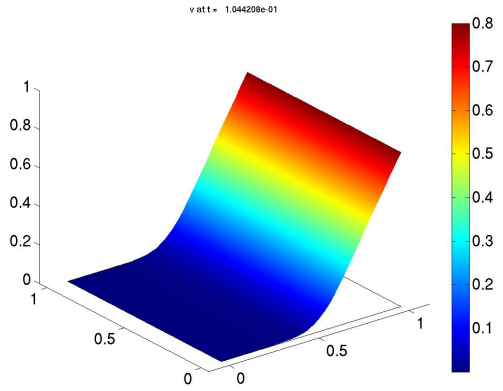

$t = 10^{-1}$

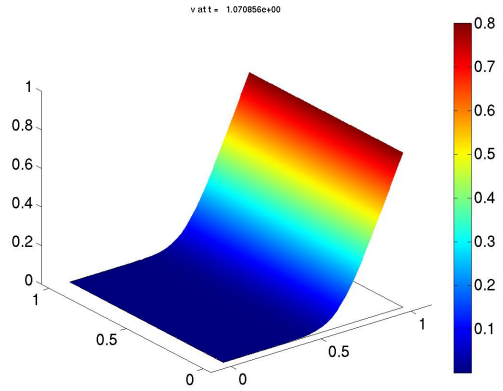

$t = 1$

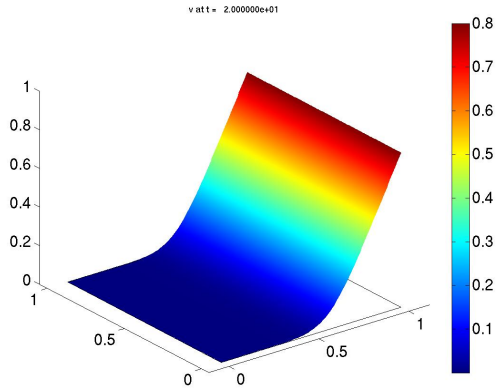

$t = 20$

Figure 3: $v(x, y, t)$ vs. (x, y) at specified times for $\lambda = 10^3$.

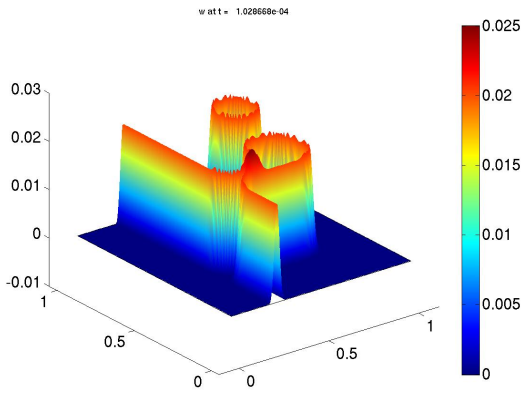

$t = 10^{-4}$

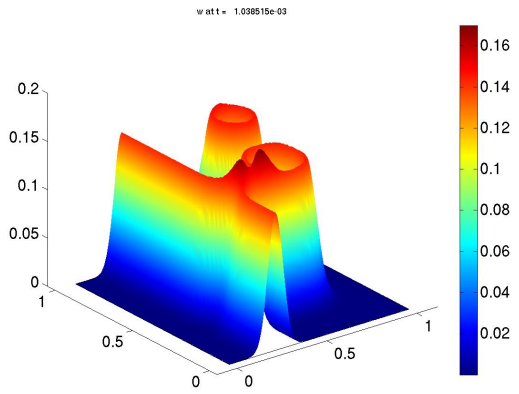

$t = 10^{-3}$

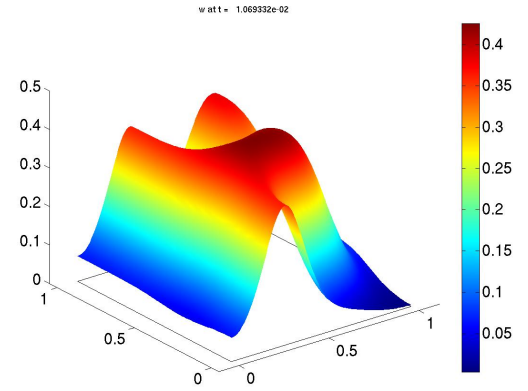

$t = 10^{-2}$

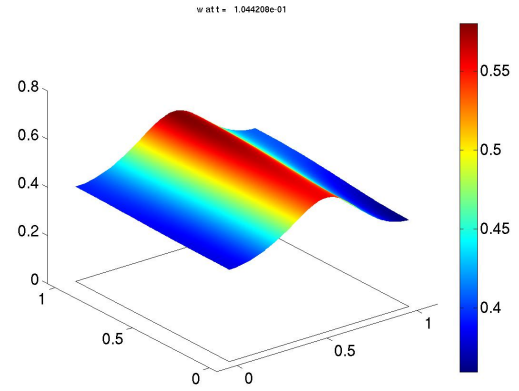

$t = 10^{-1}$

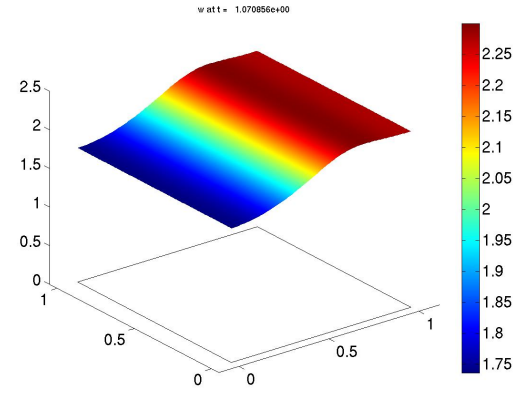

$t = 1$

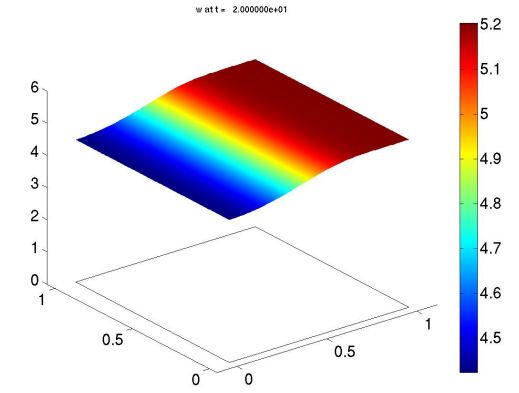

$t = 20$

Figure 4: $w(x, y, t)$ vs. (x, y) at specified times for $\lambda = 10^3$.

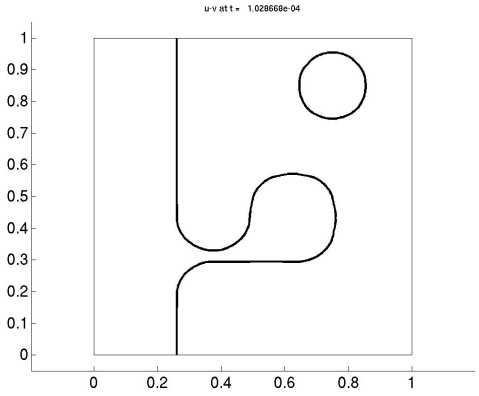

$t = 10^{-4}$

$t = 10^{-3}$

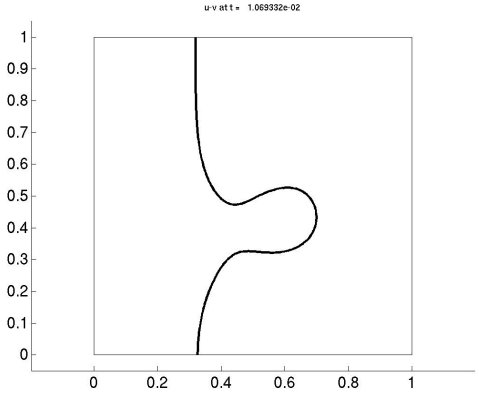

$t = 10^{-2}$

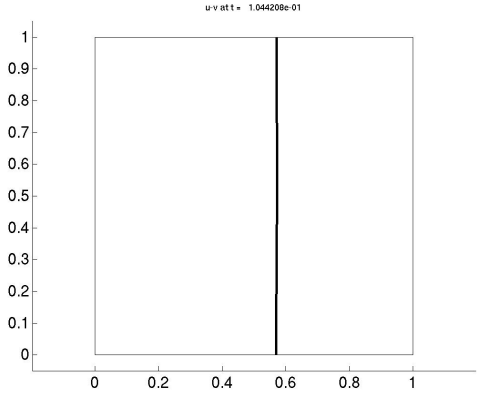

$t = 10^{-1}$

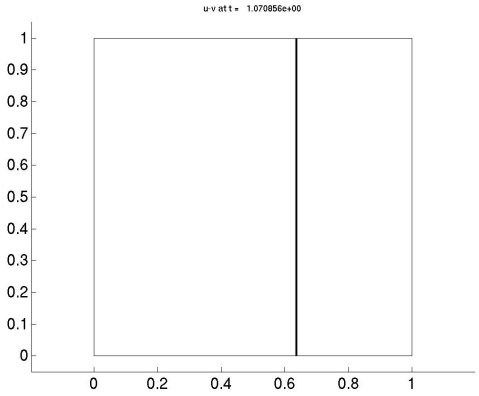

$t = 1$

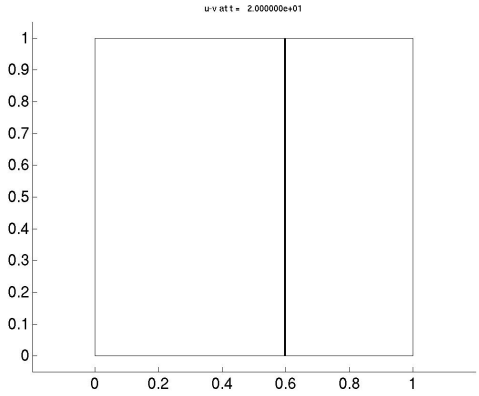

$t = 20$

Figure 5: Interface at specified times for $\lambda = 10^3$.

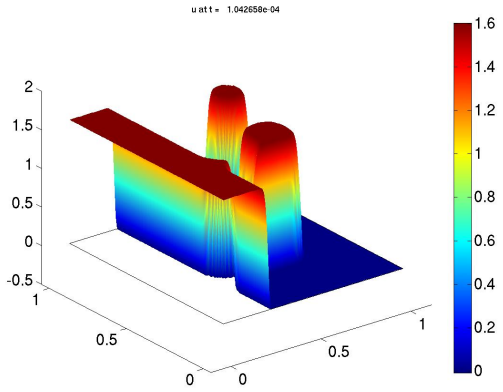

$t = 10^{-4}$

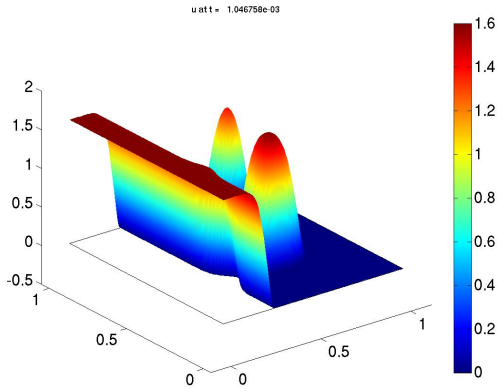

$t = 10^{-3}$

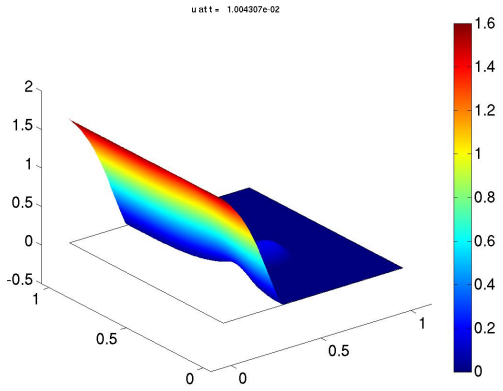

$t = 10^{-2}$

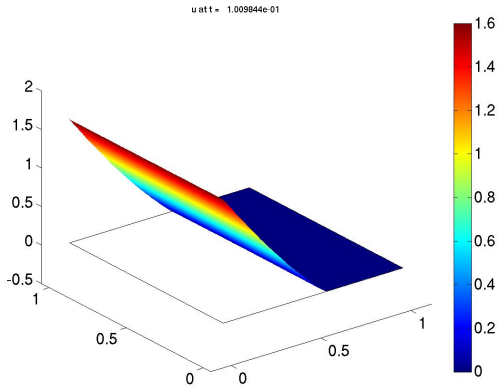

$t = 10^{-1}$

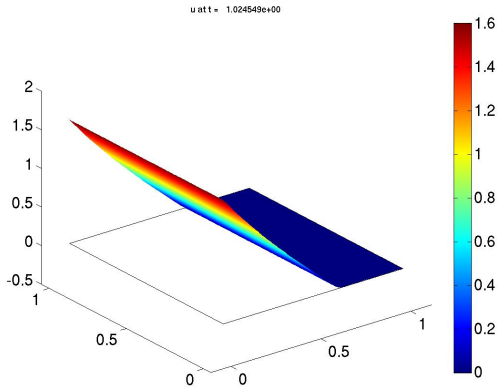

$t = 1$

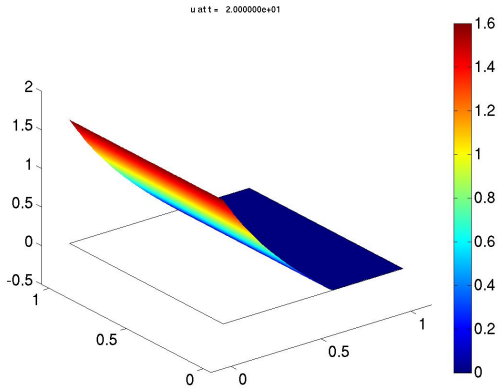

$t = 20$

Figure 6: $u(x, y, t)$ vs. (x, y) at specified times for $\lambda = 10^6$.

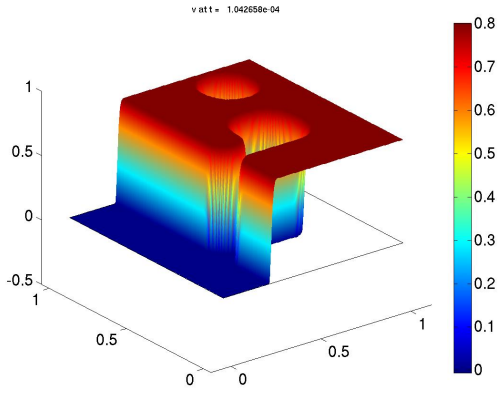

$t = 10^{-4}$

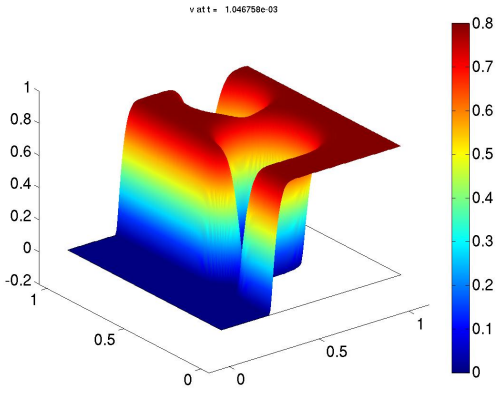

$t = 10^{-3}$

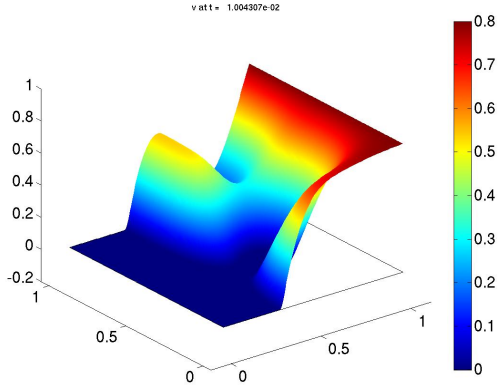

$t = 10^{-2}$

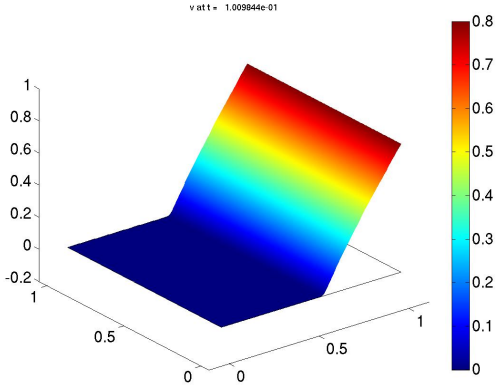

$t = 10^{-1}$

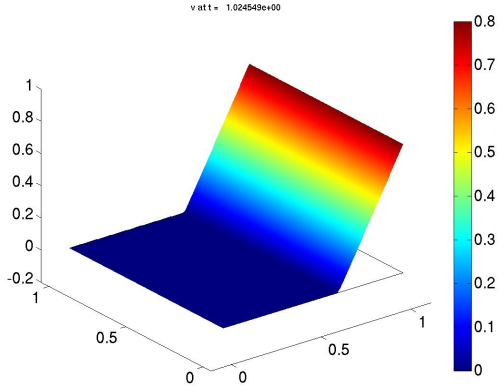

$t = 1$

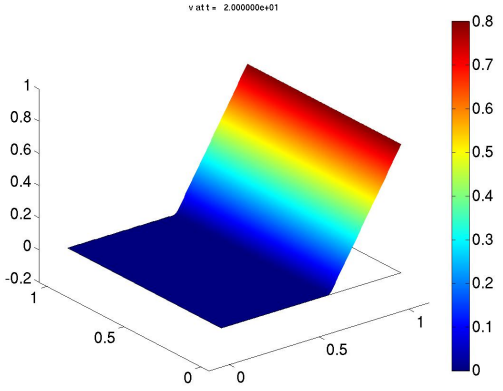

$t = 20$

Figure 7: $v(x, y, t)$ vs. (x, y) at specified times for $\lambda = 10^6$.

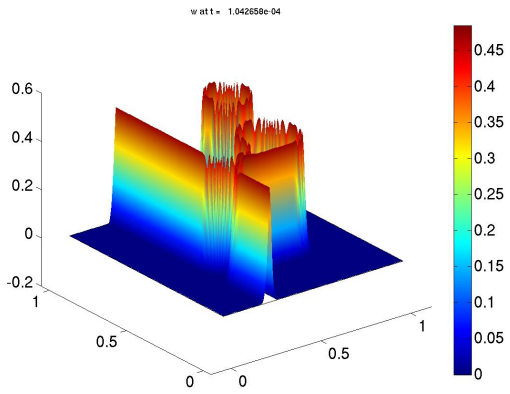

$t = 10^{-4}$

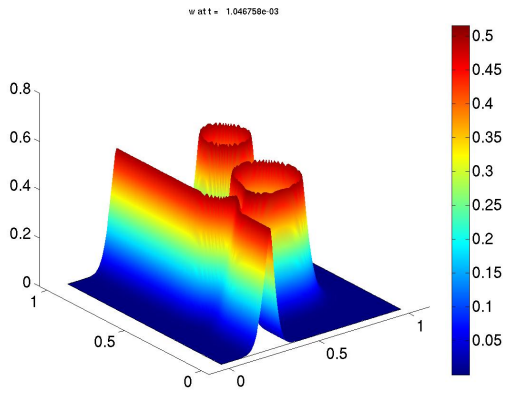

$t = 10^{-3}$

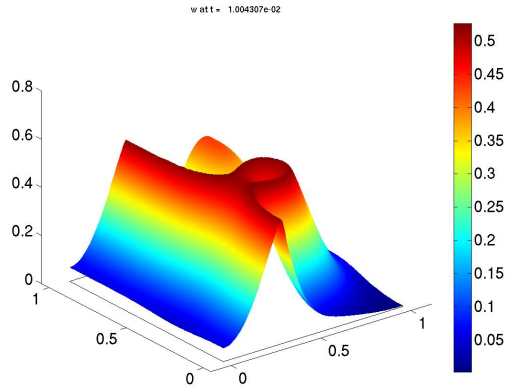

$t = 10^{-2}$

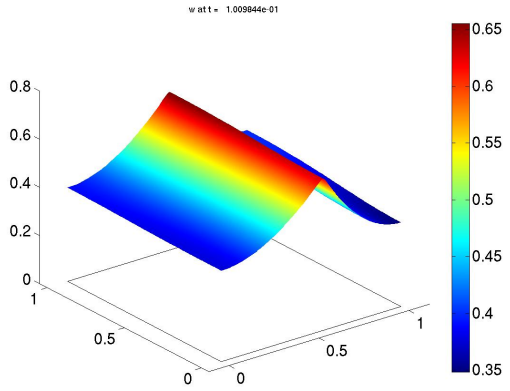

$t = 10^{-1}$

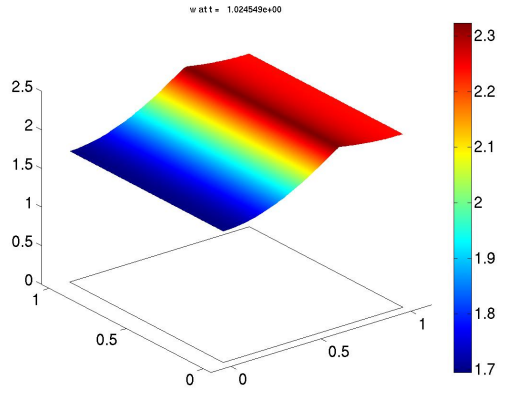

$t = 1$

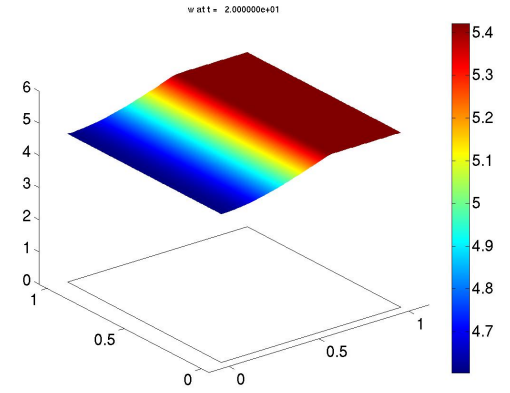

$t = 20$

Figure 8: $w(x, y, t)$ vs. (x, y) at specified times for $\lambda = 10^6$.

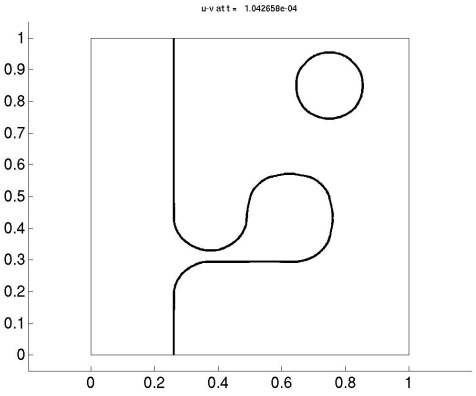

$t = 10^{-4}$

$t = 10^{-3}$

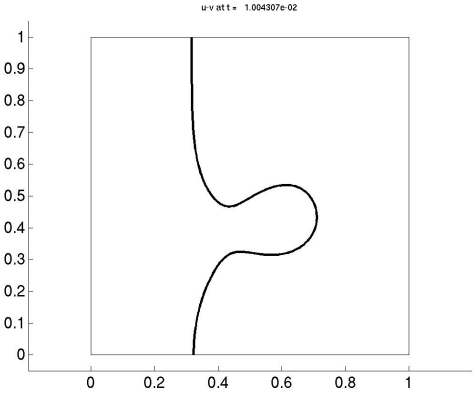

$t = 10^{-2}$

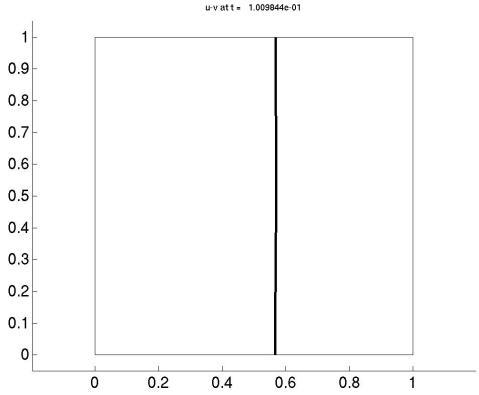

$t = 10^{-1}$

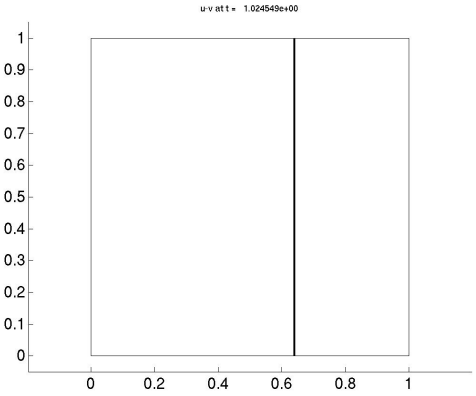

$t = 1$

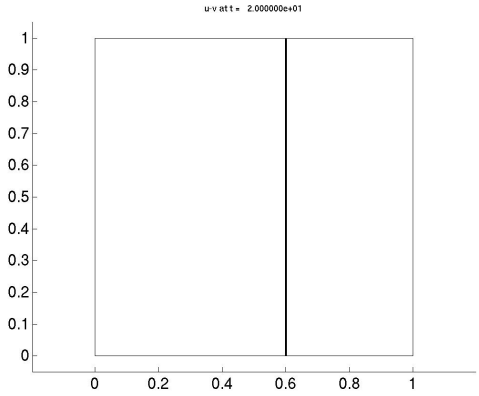

$t = 20$

Figure 9: Interface at specified times for $\lambda = 10^6$.

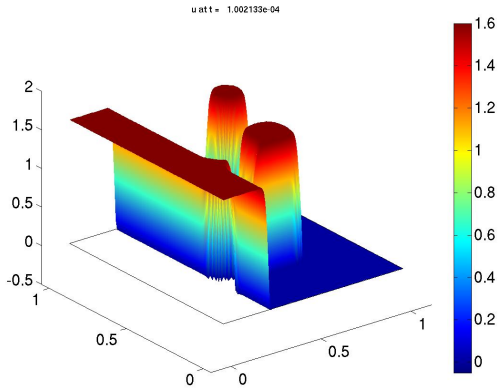

$t = 10^{-4}$

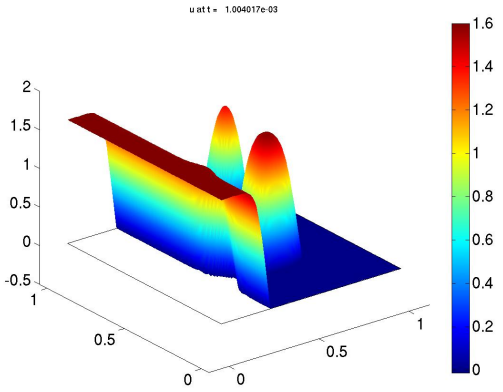

$t = 10^{-3}$

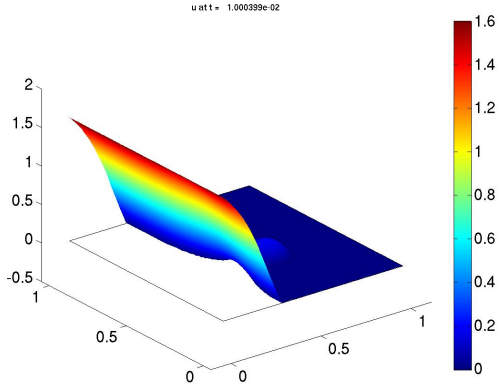

$t = 10^{-2}$

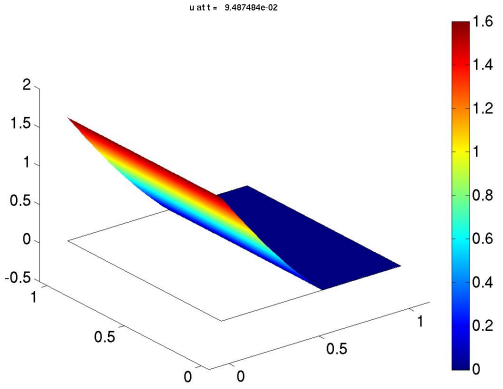

$t = 10^{-1}$

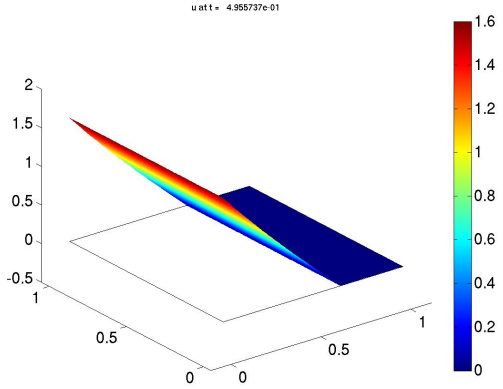

$t = 1$

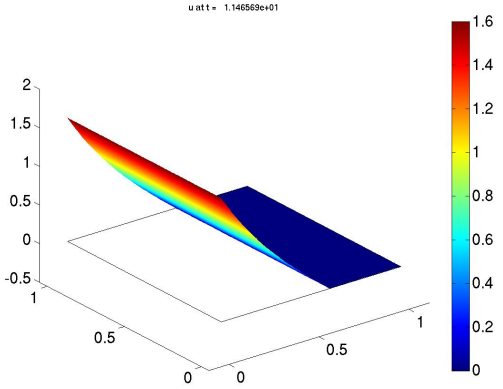

$t = 20$

Figure 10: $u(x, y, t)$ vs. (x, y) at specified times for $\lambda = 10^9$.

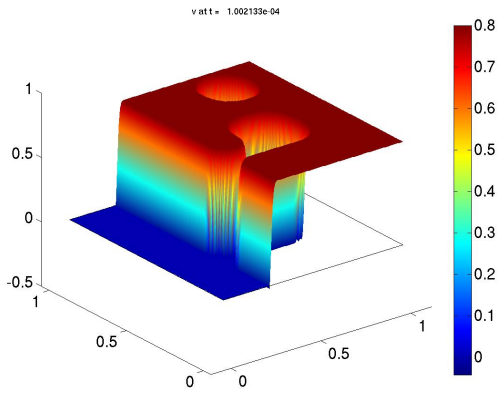

$t = 10^{-4}$

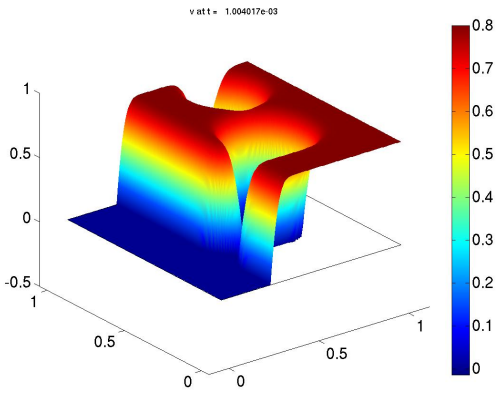

$t = 10^{-3}$

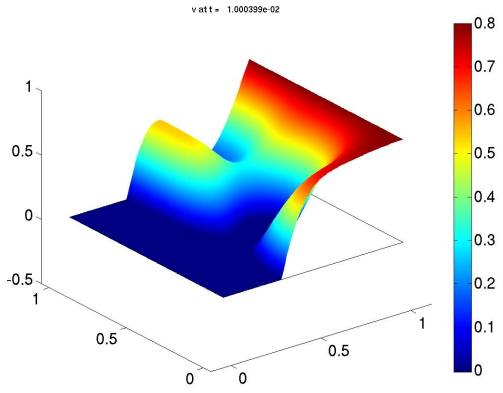

$t = 10^{-2}$

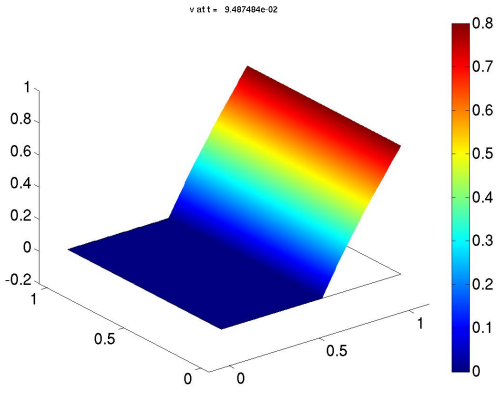

$t = 10^{-1}$

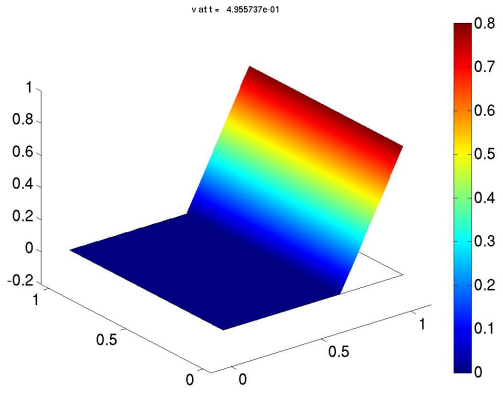

$t = 1$

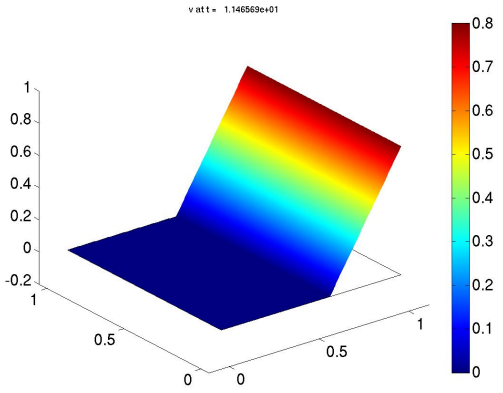

$t = 20$

Figure 11: $v(x, y, t)$ vs. (x, y) at specified times for $\lambda = 10^9$.

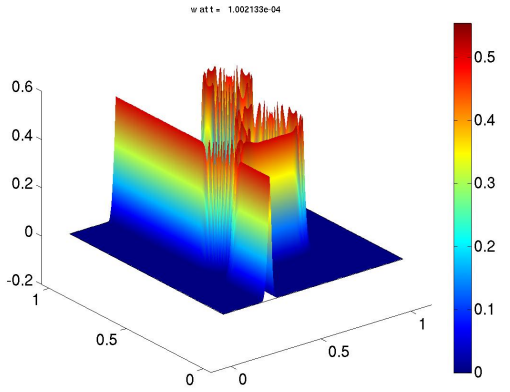

$t = 10^{-4}$

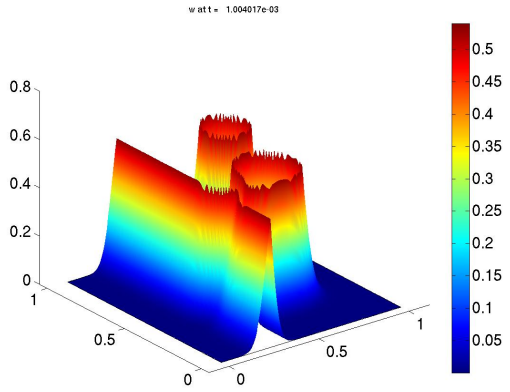

$t = 10^{-3}$

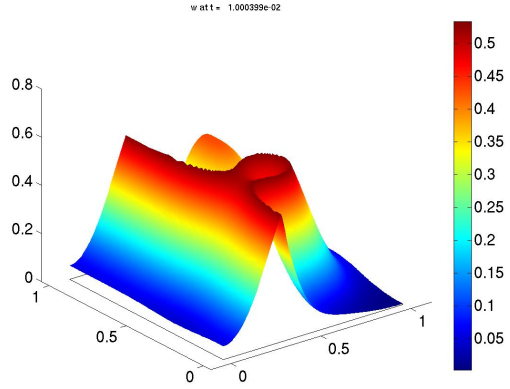

$t = 10^{-2}$

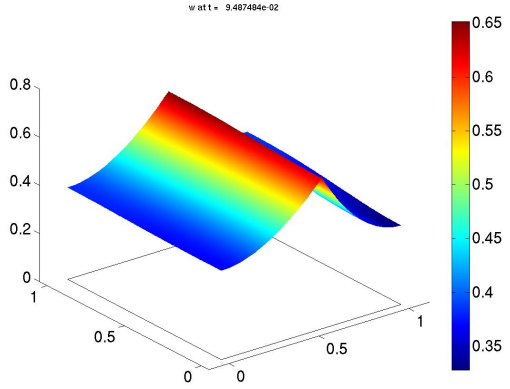

$t = 10^{-1}$

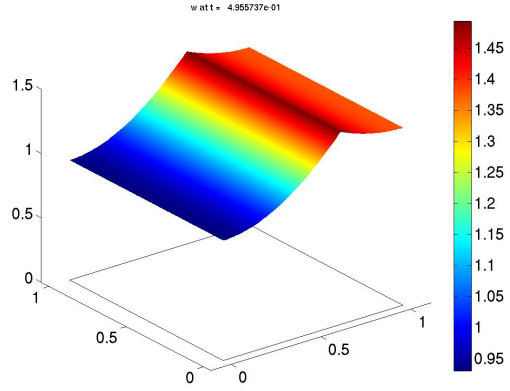

$t = 1$

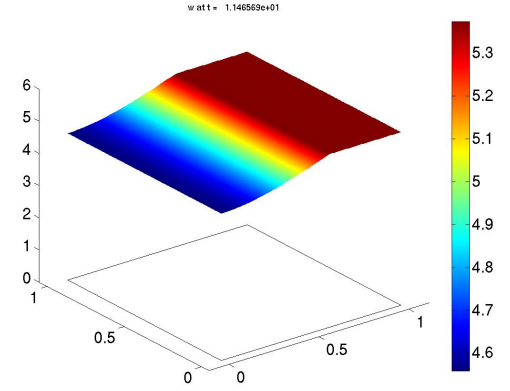

$t = 20$

Figure 12: $w(x, y, t)$ vs. (x, y) at specified times for $\lambda = 10^9$.

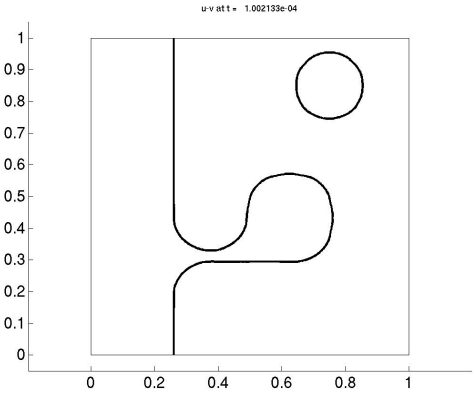

$t = 10^{-4}$

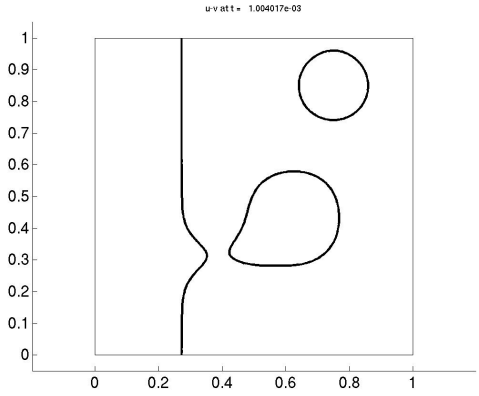

$t = 10^{-3}$

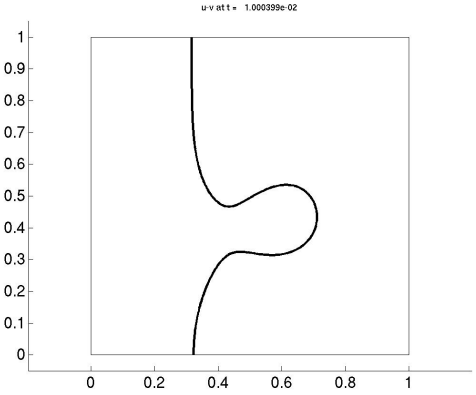

$t = 10^{-2}$

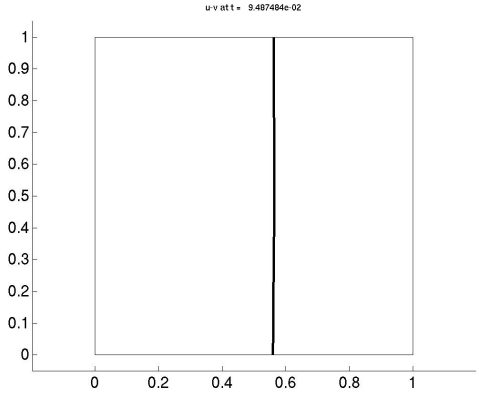

$t = 10^{-1}$

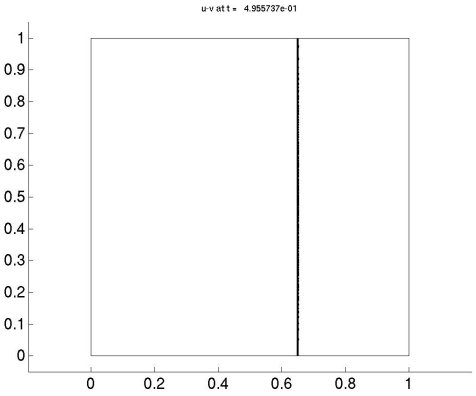

$t = 1$

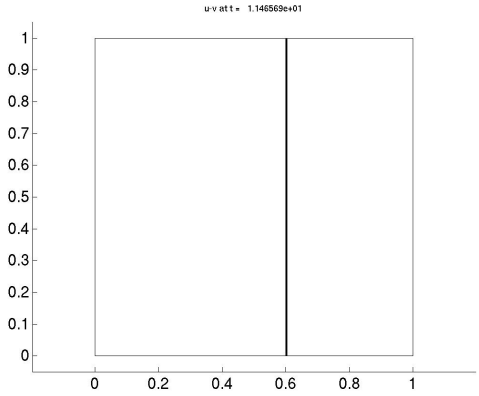

$t = 20$

Figure 13: Interface at specified times for $\lambda = 10^9$.

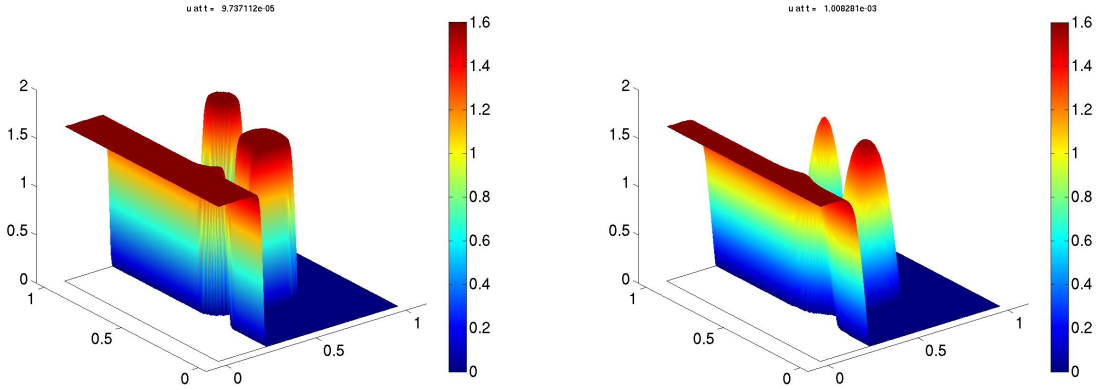

$t = 10^{-4}$

$t = 10^{-3}$

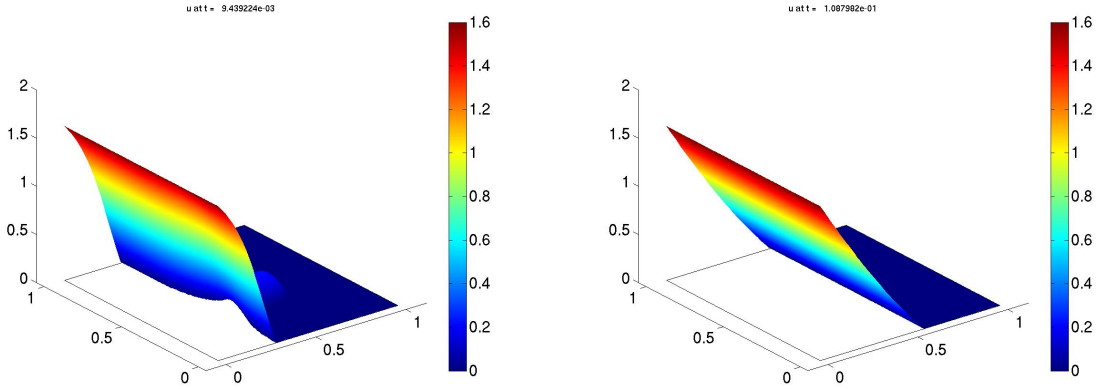

$t = 10^{-2}$

$t = 10^{-1}$

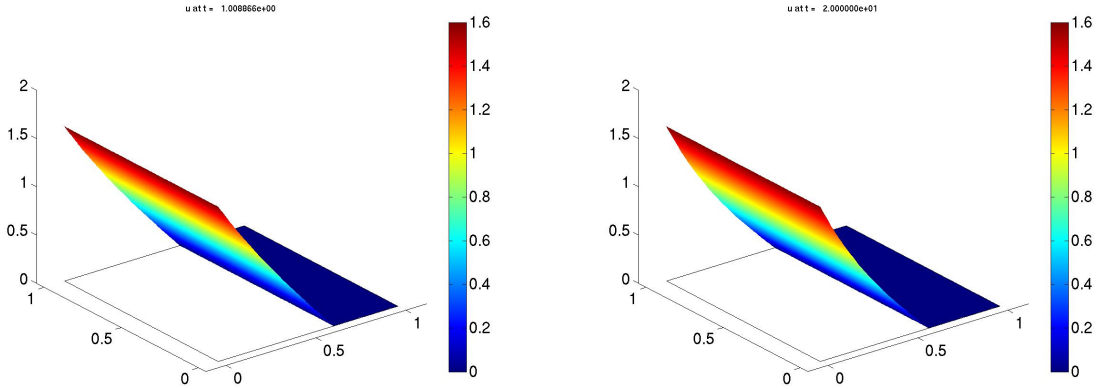

$t = 1$

$t = 20$

Figure 14: $u(x, y, t)$ vs. (x, y) at specified times for $\lambda = \infty$.

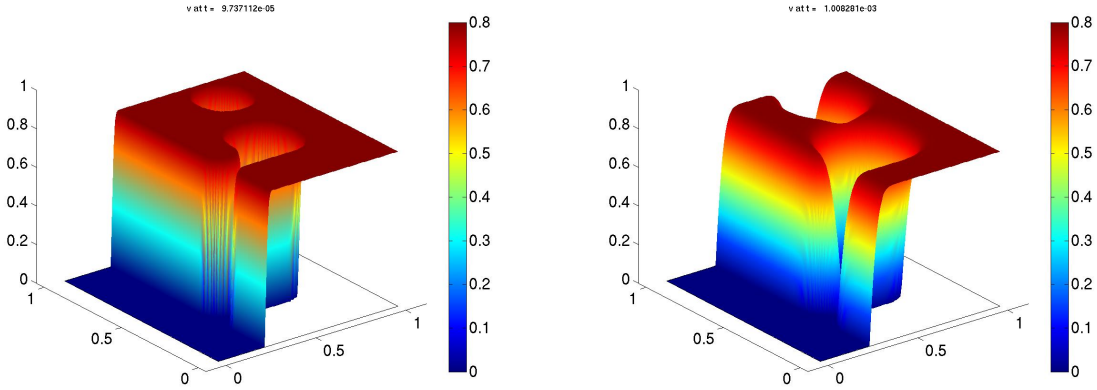

$t = 10^{-4}$

$t = 10^{-3}$

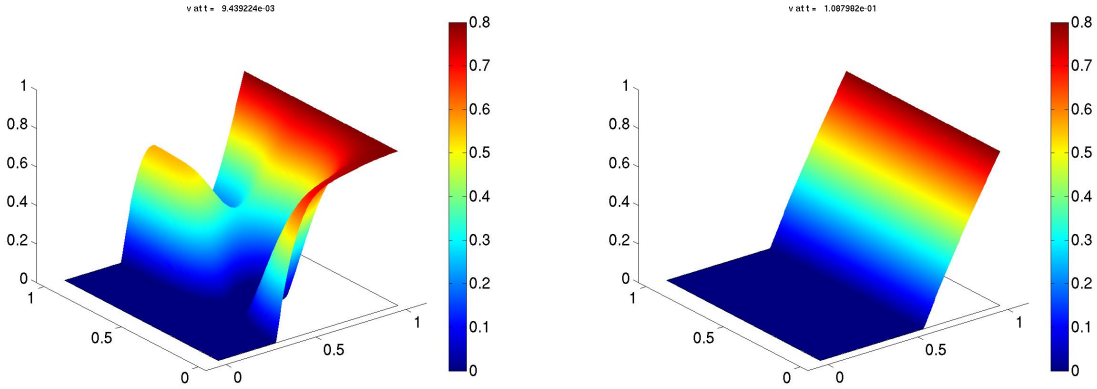

$t = 10^{-2}$

$t = 10^{-1}$

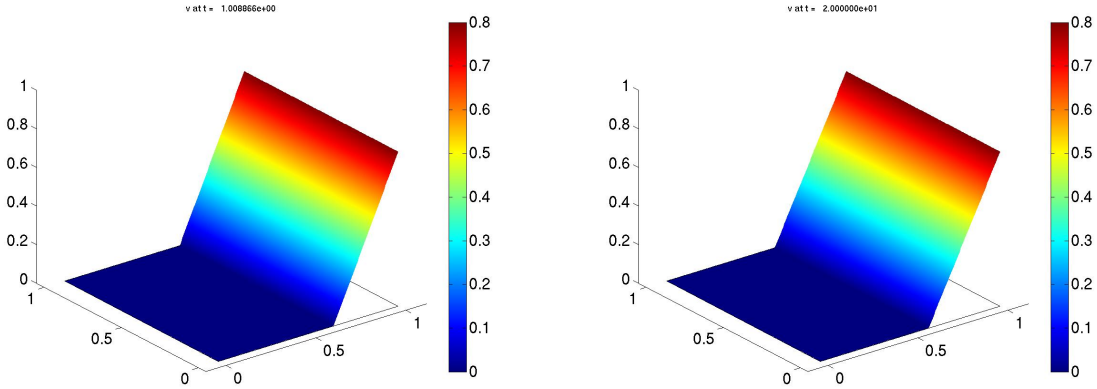

$t = 1$

$t = 20$

Figure 15: $v(x, y, t)$ vs. (x, y) at specified times for $\lambda = \infty$.

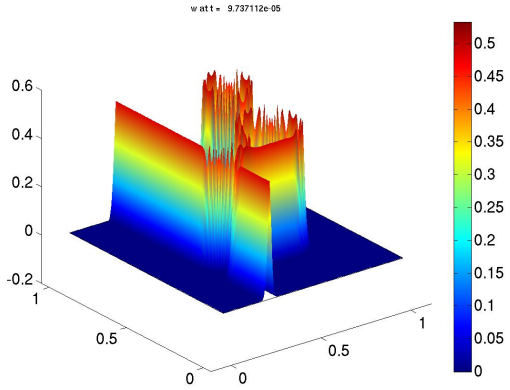

$t = 10^{-4}$

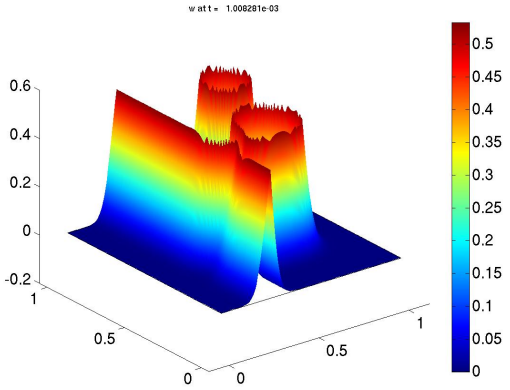

$t = 10^{-3}$

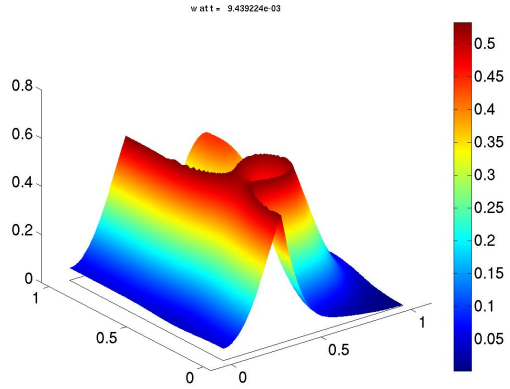

$t = 10^{-2}$

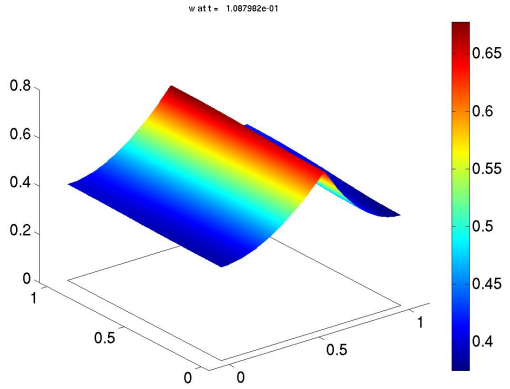

$t = 10^{-1}$

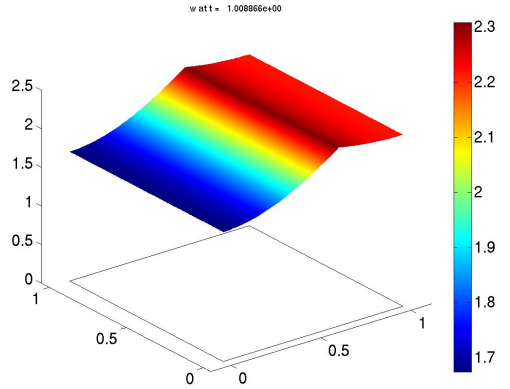

$t = 1$

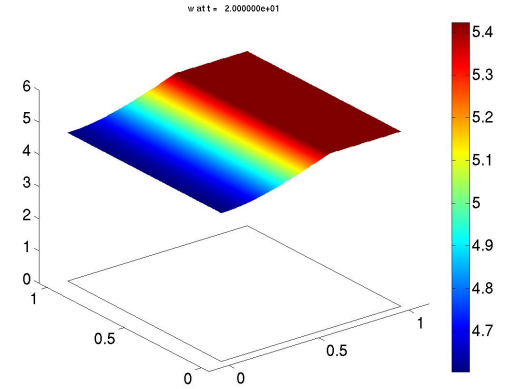

$t = 20$

Figure 16: $w(x, y, t)$ vs. (x, y) at specified times for $\lambda = \infty$.

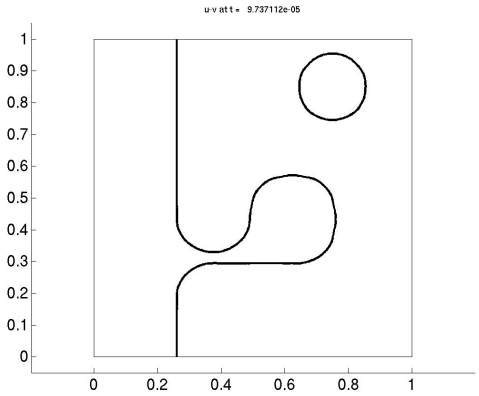

$t = 10^{-4}$

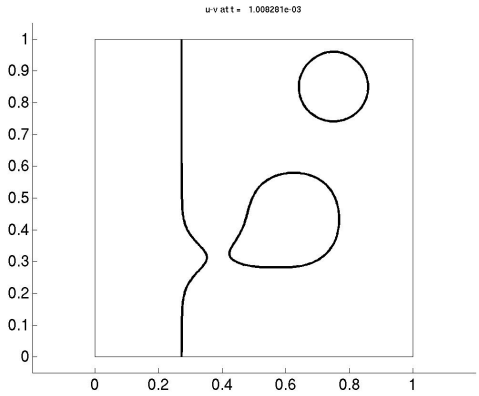

$t = 10^{-3}$

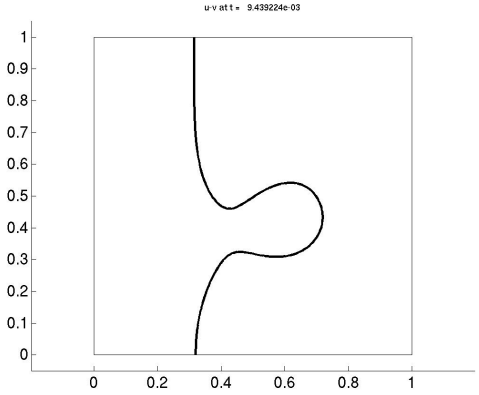

$t = 10^{-2}$

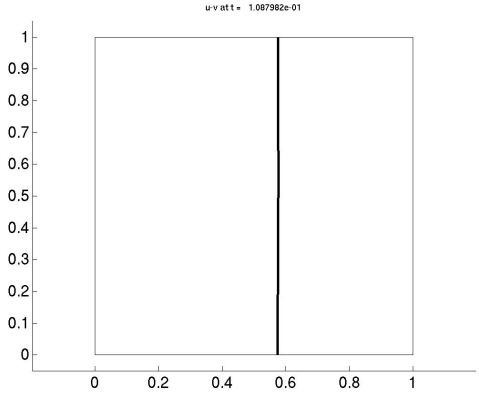

$t = 10^{-1}$

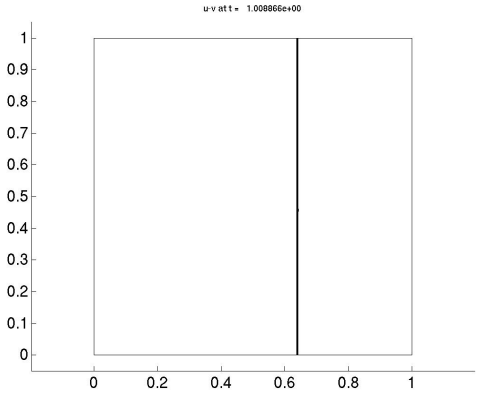

$t = 1$

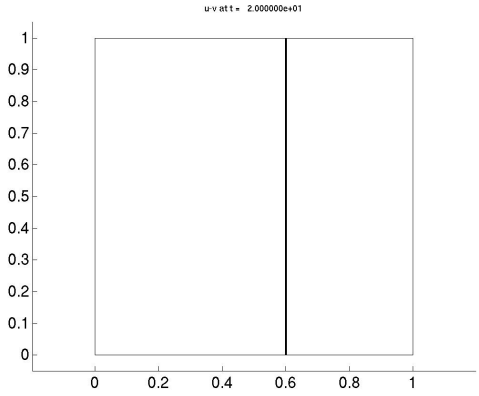

$t = 20$

Figure 17: Interface at specified times for $\lambda = \infty$.

Table 1: Summary of accuracy and efficiency data for simulations of the three species model with $\lambda = 10^3$, 10^6, and 10^9, and the two component model with $\lambda = \infty$.

$\lambda = 10^3$						
Resolution	Time to Complete (s)	Time Steps	x^*	$t_1(\times 10^{-4})$	$t_2(\times 10^{-3})$	$t_3(\times 10^{-3})$
64×64	43	215	0.609375000	1.608304	7.077499	7.077499
128×128	166	230	0.609375000	4.961102	6.354030	6.768004
256×256	771	249	0.601562500	3.716557	6.972642	6.972642
$\lambda = 10^6$						
Resolution	Time to Complete (s)	Time Steps	x^*	$t_1(\times 10^{-4})$	$t_2(\times 10^{-3})$	$t_3(\times 10^{-3})$
64×64	140	573	0.625000000	1.567014	6.863272	6.795620
128×128	467	571	0.609375000	4.831523	6.317239	6.768036
256×256	2,463	548	0.605468750	3.578299	6.753300	6.836752
$\lambda = 10^9$						
Resolution	Time to Complete (s)	Time Steps	x^*	$t_1(\times 10^{-4})$	$t_2(\times 10^{-3})$	$t_3(\times 10^{-3})$
64×64	231	646	0.625000000	1.661473	6.862192	6.790343
128×128	1,802	1,743	0.609375000	4.804291	6.267175	6.696524
256×256	11,391	2,353	0.605468750	3.612976	6.685775	6.791933
$\lambda = \infty$						
Resolution	Time to Complete (s)	Time Steps	x^*	$t_1(\times 10^{-4})$	$t_2(\times 10^{-3})$	$t_3(\times 10^{-3})$
64×64	31	203	0.625000000	1.564306	6.903623	6.903623
128×128	95	229	0.609375000	4.910450	6.459946	6.623560
256×256	444	234	0.605468750	3.619295	7.091791	7.091791

computation time in seconds taken by the COMSOL script. We see from Table 1 that the number of time steps for each λ value is on the same order of magnitude for all $N \times N$ meshes reported, except for the most numerically challenging $\lambda = 10^9$ case. The computation times get significantly larger for the finer meshes due to the larger linear systems that need to be solved in each time step. For each fixed N, as λ increases, the time of computation and the number of time steps increase rapidly for the finite λ values. But for two component model with $\lambda = \infty$ in Table 1, the number of time steps are again on the scale of the $\lambda = 10^3$ case. This indicates that the smoothness of the two component model is comparable to the three species model with this moderate λ value; the computation time is even faster than that case resulting from the smaller number of unknowns in the system for two PDEs in the two component model as compared to three for the three species model. We point out that in the case of the 64×64 mesh for $\lambda = 10^9$, the ODE solver failed to converge at the ODE tolerances stated above and used for all other cases. However, this was for a different reason than with the original ODE solver. The original solver failed to find suitable convergence for initial conditions, while in this case the solver computed until it hit a point in time where it could not compute further given the minimum time step value. Thus the data listed in the table is computed with relative and absolute ODE tolerences that are one order of magnitude coarser than the ones used for all other cases.

Taken together, because the accuracy results are nearly identical across at least $\lambda = 10^6$, 10^9, and ∞ for each fixed mesh resolution, the accuracy and efficiency measures demonstrate that the two component model ($\lambda = \infty$) is an accurate and efficient simulator for the three species model in the asymptotic limit on a given mesh.

Acknowledgments

The hardware used in the computational studies is part of the UMBC High Performance Computing Facility (HPCF). The facility is supported by the U.S. National Science Foundation through the MRI program (grant no. CNS–0821258) and the SCREMS program (grant no. DMS–0821311), with additional substantial support from the University of Maryland, Baltimore County (UMBC). See `www.umbc.edu/hpcf` for more information on HPCF and the projects using its resources.

References

[1] Leonid V. Kalachev and Thomas I. Seidman. Singular perturbation analysis of a stationary diffusion/reaction system whose solution exhibits a corner-type behavior in the interior of the domain. *J. Math. Anal. Appl.*, vol. 288, pp. 722–743, 2003.

[2] Michael Muscedere and Matthias K. Gobbert. Parameter study of a reaction-diffusion system near the reactant coefficient asymptotic limit. *Dynamics of Continuous, Discrete and Impulsive Systems Series A Supplement*, pp. 29–36, 2009.

[3] Thomas I. Seidman. Interface conditions for a singular reaction-diffusion system. *Discrete and Cont. Dynamical Systems*, to appear.

[4] Thomas I. Seidman and Leonid V. Kalachev. A one-dimensional reaction/diffusion system with a fast reaction. *J. Math. Anal. Appl.*, vol. 209, pp. 392–414, 1997.

[5] Thomas I. Seidman and Adrian Muntean. Fast-reaction asymptotics for a time-dependent reaction-diffusion system with a nonlinear source term. In preparation.

[6] Ana Maria Soane, Matthias K. Gobbert, and Thomas I. Seidman. Numerical exploration of a system of reaction-diffusion equations with internal and transient layers. *Nonlinear Anal.: Real World Appl.*, vol. 6, no. 5, pp. 914–934, 2005.

[7] Guan Wang, Aaron Churchill, Matthias K. Gobbert, and Thomas I. Seidman. Efficient computation for a reaction-diffusion system with a fast reaction with continuous and discontinuous initial data using COMSOL Multiphysics. Technical Report HPCF–2009–3, UMBC High Performance Computing Facility, University of Maryland, Baltimore County, 2009.